Journal of Wind Engineering & Industrial Aerodynamics 172 (2018) 230–243

Contents lists available at ScienceDirect

Journal of Wind Engineering & Industrial Aerodynamics

journal homepage: www.elsevier.com/locate/jweia

The effect of the ground condition on high-speed train slipstream

Shibo Wang [a,*], David Burton [a], Astrid H. Herbst [b], John Sheridan [a], Mark C. Thompson [a]

[a] Fluids Laboratory for Aeronautical and Industrial Research (FLAIR), Dept. of Mechanical Engineering, Monash University, Australia
[b] Centre of Competence for Aero- and Thermodynamics, Bombardier Transportation, Västeras, Sweden

ARTICLE INFO

Keywords:
High-speed trains
Train aerodynamics
Ground motion
Slipstream
Computational fluid dynamics (CFD)
Detached eddy simulation (DES)

ABSTRACT

Understanding the induced movement of air as a high-speed train passes (*slipstream*) is important for commuter and track-side worker safety. Slipstream is affected by the movement of the train relative to the ground, but this is difficult to include in wind-tunnel tests. Using simulations based on the Improved Delayed Detached Eddy Simulation model, this study investigates the effect of relative ground motion on slipstream for three different ground/wheel configurations: a stationary ground with stationary wheels, a moving ground with stationary wheels, and a moving ground with rotating wheels.

By examining the interaction between the train-induced flow structure and ground boundary layer, this study identifies two ways that the ground boundary layer changes slipstream: through directly altering the high slipstream velocity region due to the ground boundary-layer development, and through indirect widening of the wake by deformation of the trailing vortices. The altered aerodynamic loading on a train due to relative ground motion is visualised through the surface pressure distribution, allowing the resultant impact on drag and lift to be assessed. For wheel rotation, it is concluded that its effect is mainly restricted to be within the bogie regions, with limited influence on the wake behind the train.

1. Introduction

Slipstream quantifies the induced air movement of a high-speed train (HST) as it passes. In terms of regulations, the slipstream velocity is quantified by the resultant induced horizontal velocity in the stationary reference frame measured at a specific point or points from the train vertical centreplane. With technological development, the speed of HSTs has dramatically increased over the past decades, with typical current cruising speeds of approximately 300 km/h. Given these extreme speeds, as slipstream velocity is proportional to train speed, it can be a serious safety hazard to commuters and trackside workers, and can also cause damage to infrastructure along track lines. Because of these dangers, many countries have enforced regulations to limit the maximum permissible slipstream velocity, for example, countries in Europe through the European legislation and standards (European Union Agency for Railways, 2014; Railway Applications, 2013). Therefore, slipstream poses one of the considerations for HST design, especially if the train is to operate in the higher speed range. As the induced slipstream velocity depends on the flow development around the train and in the wake, an accurate prediction of the flow structure is essential for understanding slipstream characteristics. Compared with conventional road vehicles, HSTs have more streamlined shapes with no fixed flow separation points, a much larger length-to-width ratio, and they travel close to the ground at a significantly higher speed. Therefore, the flow around a HST is unique, and existing knowledge of neither conventional road vehicles aerodynamics nor aircraft aerodynamics can be directly utilised to understand HST aerodynamics.

Much effort has been channeled into studying train aerodynamics from many aspects, such as slipstream assessment (Bell et al., 2014), shape optimisation (Shuanbao et al., 2014), cross-wind instability (Krajnović et al., 2012) and underbody flow (Zhang et al., 2016). Similar to road vehicle aerodynamics, accurate modelling of the ground motion relative to vehicle is an important consideration. Currently, the most widely-used methods for studying HST aerodynamics are full-scale testing, moving-model testing, wind-tunnel experiments and numerical simulation. For physical experiments, full-scale and moving-model testing inherently employ a realistic ground boundary treatment, whilst in order to obtain an effective ground representation in a wind tunnel, either ground simulation techniques (such as boundary-layer suction) are essential or use of a moving-belt is recommended (Fago et al., 1991). Even though full-scale and moving-model testing utilise a more realistic stationary reference frame, the measurements are sensitive to the full-scale environmental conditions, e.g., ambient wind conditions. In any case, it is very difficult to undertake detailed measurements of the

* Corresponding author.
E-mail address: shibo.wang@monash.edu (S. Wang).

https://doi.org/10.1016/j.jweia.2017.11.009
Received 1 June 2017; Received in revised form 16 October 2017; Accepted 10 November 2017

flow field around a moving model and to conduct unsteady statistical analyses, such as flow mapping of the mean or phase-averaged wake.

In contrast, wind-tunnel experiments adopt the vehicle reference frame, making it much easier to undertake measurements of the flow structure around the train model and in the wake. In general, it is both difficult and expensive to equip a wind tunnel with a moving floor for train aerodynamics research.

Compared with conventional road vehicles, HSTs typically have a much larger length-to-height ratio, typically around $50 \sim 100$. Additionally, HSTs appear to have a longer coherent wake structure than road vehicles. For example, the region of interest for road vehicles is typically within 3 vehicle heights, since drag is the primary consideration, while the region of interest for HST slipstream assessment can be up to $5 \sim 10$ train heights behind the tail because sideways wake movement/oscillation can have a strong effect on slipstream. For example, Bell et al. (2017) reported that the train wake disturbance was significant up to around 20 train heights (the peak slipstream velocity was recorded at approximately $5 \sim 10$ train heights) behind the tail according to the wind tunnel, moving model rig and full-scale testing experiments, all based on an ICE3 train model. As a consequence, even if a moving floor is implemented, a significantly longer moving-belt is required to represent the relative motion, not only along the long train but also in the extended wake region. Additionally, according to the CEN guidelines (Railway Applications, 2013), the aerodynamic performance of a HST needs to be studied not only on a flat ground configuration, but also on an elevated ballast configuration. The introduction of a moving ballast makes employing a moving-belt technique almost impossible for wind-tunnel experiments. Therefore, understanding the potential differences that can be introduced by adopting a stationary floor is essential.

Relative to HSTs, the effect of incorrect relative ground motion has been extensively studied for road vehicles. The previous research of the underbody flow with different ground conditions have shown that the moving ground configuration can increase the mass flux underneath the vehicle in the streamwise direction and decrease it in the spanwise direction, and this alters the aerodynamic loading on the underbody structure (Krajnović and Davidson, 2005). However, different studies with different geometries, do not provide a consistent trend on the aerodynamic loading and flow. For example, Krajnović et al (Krajnović and Davidson, 2005) reported that floor motion reduced drag by 8% and lift by 16% on a simplified car with a typical fastback geometry, while Burgin et al. (1986) found an increase in drag for flow past a bluff body with a moving ground. Additionally, Sardou (1986) found a significant alteration to the rear wake with/without ground motion, while Krajnović et al (Krajnović and Davidson, 2005) found that the wake flow was relatively insensitive.

For future development of HSTs, a fuller understanding of the flow around and behind a HST is becoming more important, and to achieve that the inclusion of an accurate ground boundary condition would seem important. If this is not possible, an understanding of at least the semi-quantitative effects that can be caused by different ground motion configurations would seem necessary.

Some previous research has been channelled into investigating the effect of ground motion. Kwon et al. (2001) studied the performance of two ground simulation techniques, a moving-belt system and a tangential blowing system, based on a Korean HST. The results showed that a moving floor could increase the aerodynamic drag by approximately 15%, and this was explained as the result of the increase in both friction and pressure drag. Specifically, the altered boundary-layer profile beneath the train increased the friction drag on the train underbody, and the pressure drag was increased due to the stronger vortical wake structures. Xia et al. (2016a,b), compared the effect of a stationary and moving ground on the flow structure and aerodynamic loading on a Chinese HST (CRH3) on a flat ground configuration using CFD. An identical dominant wake structure was determined for both cases, while the moving ground case showed a narrower wake with slower vortex shedding, as compared to the one with a stationary ground. Additionally, a significant variation to underbody pressure was identified due to the ground motion, which resulted in a large deviation for drag and lift predictions between stationary and moving grounds, and raising the train model, which was thought might reduce differences, could not effectively eliminate this variation. Zhang et al. (2016) further examined the combination effect of the ground motion and wheel rotation on underbody flow and aerodynamic loading. They found that the moving ground case showed a higher total drag on the train compared with stationary ground; however, the application of rotating wheels did not show an identifiable further increase in drag. Additionally, the impact of rotating wheels was only seen on the local pressure distribution within the bogie region, and showed as an increase of the drag of the wheels. A moving ground with rotating wheels boundary condition was concluded as necessary, especially for studying the underbody flow of a HST.

According to previous research, the ground motion has been verified to have a significant effect on the HST aerodynamic loading and the surrounding flow field. Even though the effect of the ground motion has been identified and partially investigated, a comprehensive understanding of the mechanism on how it alters the train slipstream development is yet to be undertaken and this has motivated the present study.

Indeed, the aim of current study is to investigate the effect of the ground motion on the slipstream development around a generic HST model, including identifying the mechanism by which it alters the flow structure around the train and within the wake region. Additionally, the effects of ground motion on slipstream assessment and aerodynamic loading are studied. Specifically, for a systematic comparison and determination of the effect introduced by the ground motion and the wheel rotation, three cases with different ground/wheel motions are studied: (i) Stationary Ground with Stationary Wheels (SGSW), (ii) Moving Ground with Stationary Wheels (MGSW) and (iii) Moving Ground with Rotating Wheels (MGRW).

This paper is structured as follows. The numerical set-up, including defining the train geometry, the computational domain and corresponding boundary conditions, the meshing strategy, the turbulence models and solver settings, are introduced in the *Methodology* Section. In the *Results and Analysis* section, the effect of ground motion is studied from the following three perspectives: slipstream assessment (Section 3.1), flow structure (Section 3.2), and aerodynamic loading (Section 3.3). In Section 3.1, the slipstream assessment is implemented under the TSI specifications (European Union Agency for Railways, 2014), including the analysis of unsteady statistics of the slipstream velocity profiles and gust phenomenon. Additionally, the flow field at the slipstream measurement location is investigated to reveal the mechanism on how ground motion alters the slipstream measurement. In Section 3.2, further investigations of the ground motion effect on the flow structures are conducted. For explicitly studying the ground motion effect at each stage of train slipstream development, the overall flow field is divided into two regions: the flow development region and wake propagation region. The altered aerodynamic loading is visualised through the train surface pressure distribution, and the resultant force variation (drag and lift) is presented in Section 3.3. The findings are summarised in Section 4.

2. Methodology

2.1. Geometry

The geometry used for this study was based on a Deutsche Bahn InterCity-Express 3 (ICE3) high-speed train, a widely operated train model in Asian and European countries. ICE3 has a representative external shape, and its Computer-Aided Design (CAD) model is freely available from the DIN Standards Railway Committee (FSF) (DIN, 2014). This makes ICE3 an ideal model for generic HST aerodynamic research, and a comparison between the full-scale ICE train and numerical model is illustrated in Fig. 1. Important geometric features that have a strong influence on the slipstream are retained, i.e. the bogies and snowploughs, although the CAD model is simplified. Geometric features like pantographs (Ambrósio

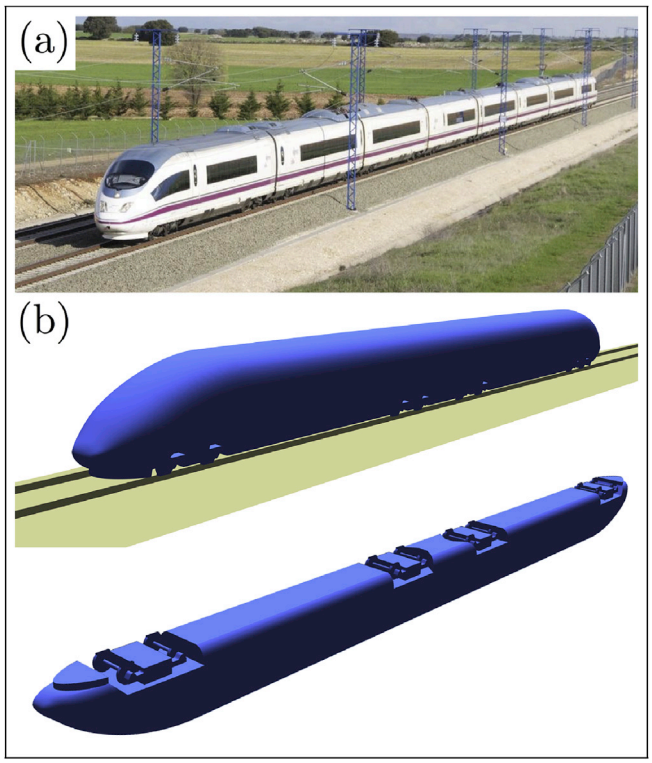

Fig. 1. Comparison between the full-scale ICE train and numerical model: (a): full-scale operational ICE3 train; (b): simplified numerical model. (Photo provided courtesy of Bombardier Transportation).

et al., 2012) and inter-carriage gaps (Mizushima et al., 2007) that have also been shown to interfere with the flow around a HST (e.g. the boundary-layer development) are omitted. The length-width-height ratio of the train model is approximately 50:3:4. The train is located on a Single Track Ballast and Rail (STBR) ground configuration, with the dimensions specified in CEN guidelines (Railway Applications, 2013). The rails are modelled by slender rectangular cross-section cylinders extruded through the entire domain, and the width of the rails is extended from 50 mm to the wheel width of 135 mm (in full-scale) in order to represent a realistic contact between the rails and wheels.

2.2. Domain and boundary conditions

The train is positioned in the centre of a hexahedral computational domain, as illustrated in Fig. 2. The origin of the coordinate system is positioned in the spanwise mid-plane, at the height of the top surface of the rails, with $x = 0$ corresponding to the tail tip.

To determine the effect of ground motion on HST slipstream, three cases are studied: SGSW, MGSW and MGRW, as described in the introduction. The geometry and solver settings for the three cases are identical, except for the boundary conditions at the ground (including the ballast and rails) and wheel sets (including the wheels and axles), which are listed in Table 1.

In order to replicate the splitter plate introduced to remove the floor boundary layer in the wind-tunnel experiments (Bell et al., 2014), the ground is split into two parts named ground 1 and ground 2. When the no-slip moving wall condition is applied to the ground surface, both ground 1 and ground 2 move horizontally at the freestream velocity of U_∞. This is to simulate the realistic condition of a moving train travelling through still air where there is no relative motion between the air and ground. For the rotating wheel sets, the axes of rotation are along the centrelines of the axles. The wheel sets rotate at a constant angular velocity, with the speed at the rim equal to the speed of the moving ground. SGSW represents a typical wind-tunnel experimental condition without a moving-belt, while MGRW is more realistic for full-scale and moving-model tests. To have a more complete study of ground motion effect, an additional case, MGSW, is studied to isolate the effect of wheel rotation.

The conditions for other boundaries are identical for the three cases. Stationary no-slip wall boundary conditions are applied to all train surfaces, other than the train wheels. A uniform velocity boundary condition with a turbulence intensity of 1% is applied at the inlet. The Reynolds number (based on W) is 7.2×10^5. These values are chosen for consistency for comparison with wind-tunnel experiments (Bell et al., 2016a,b), noting that they are not representative of full-scale train operation. A zero static pressure condition is applied at the outlet boundary. Symmetry boundary conditions are applied at the top and sides of the computational domain.

2.3. Meshing strategy

The general meshing strategy is based on the predominately-Cartesian cut-cell approach, allowing substantially increased mesh concentration around the train and in the wake, together with a relatively smooth transition to lower resolution away from the train. In particular, it achieves a high uniform resolution in the slipstream measurement regions, and aids in accurately capturing the boundary layers and induced flow separation from smaller-scale geometrical features. To ensure that all important flow features are captured, the dimensions of the refinement regions are determined based on a preliminary

Table 1
Boundary conditions of the ground and wheel sets.

Boundary conditions	SGSW	MGSW	MGRW
Ground 1	Zero-shear stationary wall	No-slip moving wall	No-slip moving wall
Ground 2	No-slip stationary wall	No-slip moving wall	No-slip moving wall
Wheel sets	No-slip Stationary wall	No-slip stationary wall	No-slip rotational wall

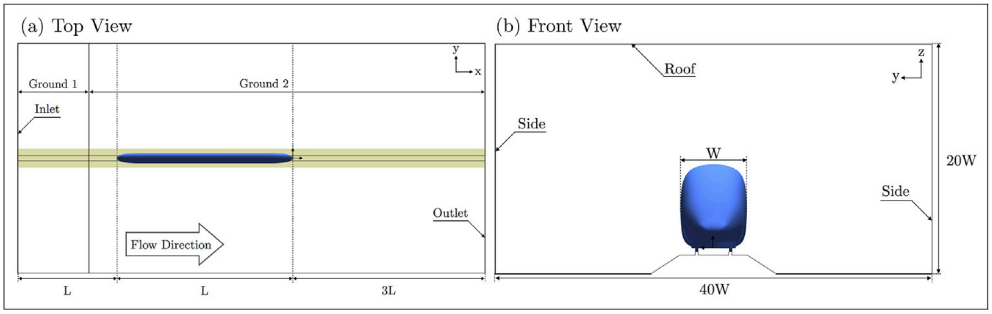

Fig. 2. Schematic of computational domain: (a): top-view; (b): front-view. (Not to scale).

simulation. Prism-layer cells are applied to all wall boundaries to capture the boundary-layer development. A smooth transition is established between the adjacent cells including between the outer inflation layers and the hexahedral grid, and at the interface of two refinement zones, as shown in Fig. 3. A mesh independence study was undertaken in a previous related study (Wang et al., 2017) examining the effect of turbulence models on slipstream prediction. In that study, the performance of three sequentially refined grids (coarse, medium and fine) for predicting HST slipstream were evaluated, showing that drag and slipstream predictions varied by less than 1% and 2% between the fine and medium grids. This study adopts the equivalent mesh settings of the fine grid, with the key meshing parameters listed in Table 2.

Table 2
Key meshing parameters.

Cell size	Train surface mesh	$0.00625H \sim 0.025H$
	Under-body refinements	$0.00625H \sim 0.0125H$
	Wake refinements	$0.0125H \sim 0.05H$
	Far-field refinements	$0.1H \sim 0.4H$
No. of inflation layers		10
Train surface wall y^+		$1 \sim 20$
No. of cells (millions)		27

2.4. Solver description

The numerical solver utilised in this research is the commercial CFD code FLUENT, which is part of the ANSYS 16.2 software suite. A pressure-based transient solver is utilised for predicting the highly turbulent flow phenomenon.

To start with, the flow field is initialised with a second-order accurate steady-state RANS simulation based on the Shear-Stress Transport (SST) RANS model. Subsequently, the flow is solved with the Improved-Delayed Detached Eddy Simulation (IDDES) turbulence model. IDDES is a type of DES model that applies an improved delayed shielding function to achieve a higher accuracy and more realistic physical behaviour within the RANS-LES blending region, which also improves the wall-modelling capability. Similar to the classic DES blend technique, IDDES also utilises a RANS model to approximate the boundary layer and applies LES to capture the time-dependent flow away from the boundaries. IDDES has been extensively adopted to study the train aerodynamics, for example, the study of the slipstream assessment (Huang et al., 2016) and underbody flows (Zhang et al., 2016). The Shear-Stress Transport (SST) $k-\omega$ model is used for the RANS component within the IDDES model, due to its superior performance on modelling the near-wall boundary-layer regions with undefined separation points. A fuller description of the IDDES model is given in (Spalart, 2009).

A timestep of $0.0025T_{\text{ref}}$ was chosen because this restricts the Courant number ≤ 1 for the typical smallest cells, which is one of the suggested criteria for conducting DES/LES simulations. Here, $T_{\text{ref}} = H/U_{\infty}$, defines a reference time for fluid to travel one train height at the background velocity. As the typical Courant number is less than unity, the non-iterative fractional-step scheme is applied. For the spatial discretisation, the second-order upwind scheme is used for the convective terms in the turbulence equations, while the bounded central-difference scheme is used for the momentum equation. Additionally, the bounded second-order implicit formulation is used for time-advancement for the transient simulations.

Unsteady statistics are obtained by averaging the flow after it was first checked to have reached its asymptotic state. This was checked through comparisons with predictions based on smaller averaging periods. Unsteady statistics are gathered over 195 T_{ref}, which is equivalent to three times the time taken for the freestream flow to advect through the entire domain from inlet to outlet, or approximately 15 times the time taken for the flow to advect the length of the train.

2.5. Validation

The SGSW case was validated against a wind-tunnel experiment in a related study (Wang et al., 2017), and good agreement was seen for important slipstream characteristics like slipstream velocity profiles, time-averaged flow topology, wake dynamics and aerodynamic loading. The wind-ltunnel experiment was conducted in the Monash University 1.4 MW closed-circuit wind tunnel, and a full description of the experimental set-up and results can be found in (Bell et al., 2017). That study comprehensively evaluated the key numerical settings (including the choice of turbulence model, grid resolution and solver time-step) for predicting the slipstream, and provided guidelines for turbulence modelling choices depending on the output parameters required. This study utilised the optimal numerical settings for time-dependent predictions derived from that study. The MGSW and MGRW cases can be considered to have similar or even slightly less complicated flows, for instance, a moving ground eliminates the ground boundary-layer development compared with SGSW. Therefore, it is appropriate to assume the optimised settings for the SGSW case are appropriate for the MGSW and MGRW cases. Additionally, the time-averaged slipstream profiles previously obtained from the wind-tunnel experiments are used for further validation.

3. Results and analysis

3.1. Slipstream assessment

Slipstream assessment is a part of the HST acceptance procedure, and this study is implemented following the European Regulations and Standards (European Union Agency for Railways, 2014; Railway Applications, 2013). Slipstream is described as the induced flow turbulence of a HST according to the ground-fixed (GF) reference frame, while the

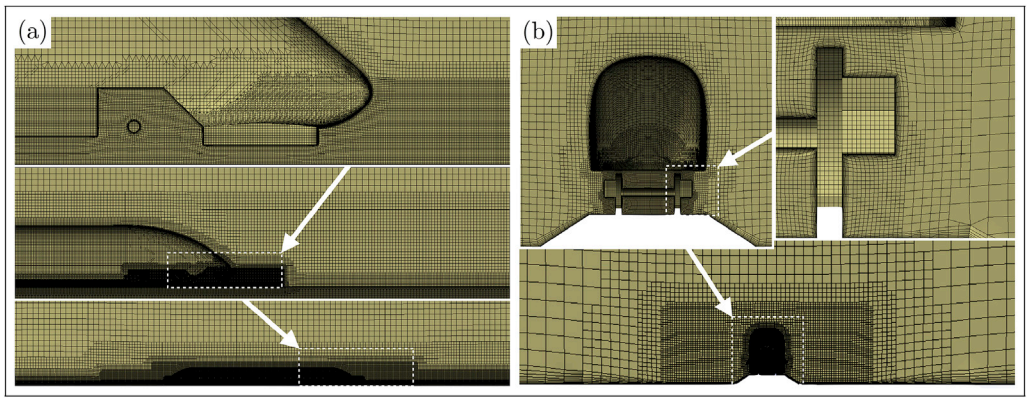

Fig. 3. The mesh refinements around the train: (a): centre-plane; (b): cross-section.

numerical simulation is based on a train-fixed (TF) reference frame; this necessitates a change of reference frame. Slipstream is quantified through the slipstream velocity field ($U_{slipstream}$), given by

$$U_{slipstream} = \sqrt{(U_{GF}^2 + V_{GF}^2)}, \quad (1)$$

where

$$U_{GF} = \frac{U_\infty - U_{TF}}{U_\infty}, V_{GF} = \frac{V_{TF}}{U_\infty}. \quad (2)$$

According to Equations (1) and (2), $U_{slipstream}$ is only based on the downstream (U) and transverse (V) components of the velocity, but not the vertical velocity component. Also note that velocities, including slipstream velocities, quoted in this study are typically normalised by the freestream velocity (U_∞).

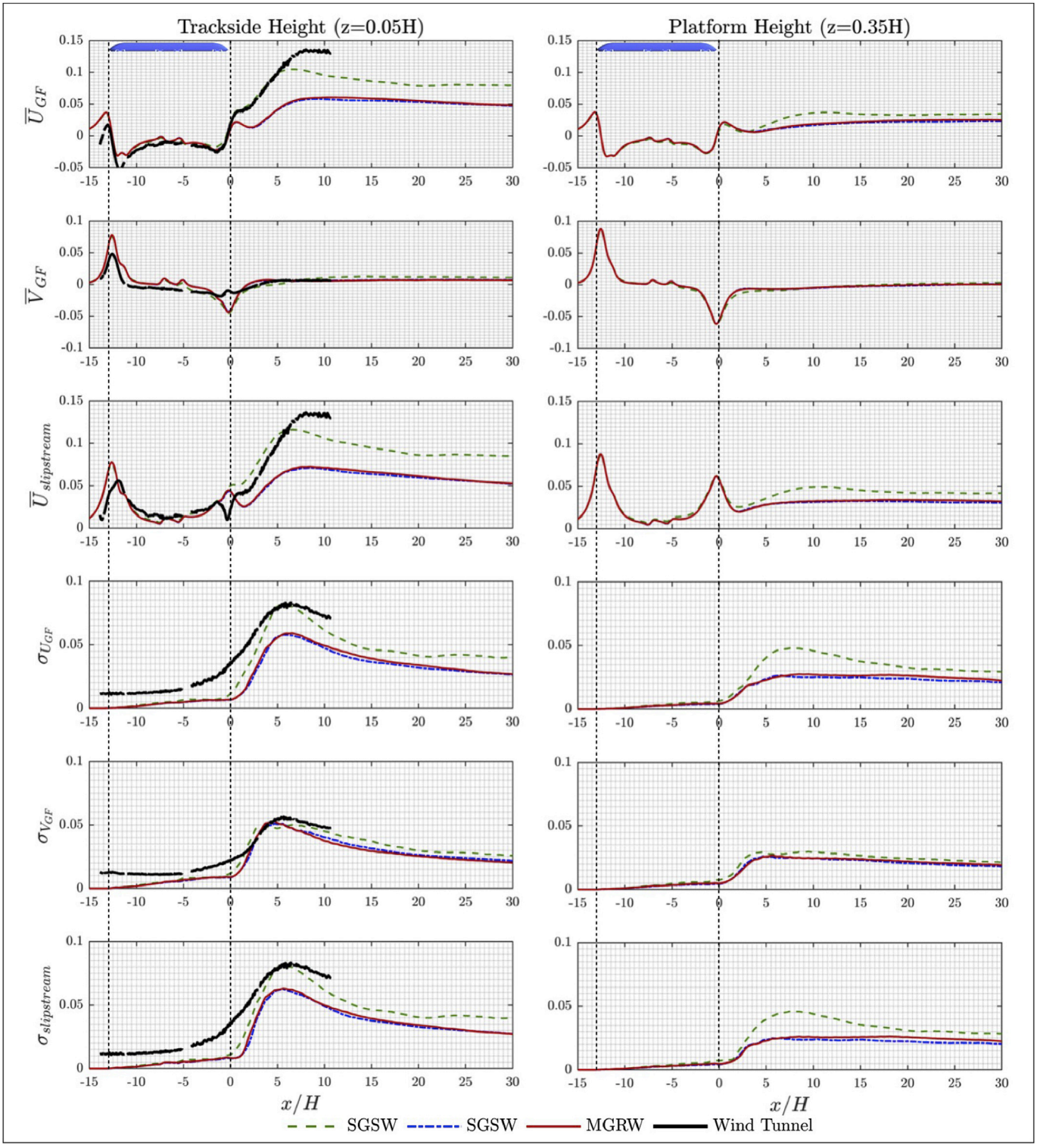

Fig. 4. The comparison of the slipstream profiles between SGSW, MGSW and MGRW at the trackside and platform heights. The wind-tunnel measurements at the trackside height are used for validation against SGSW configuration (Bell et al., 2017).

To understand the effects of ground motion on the slipstream velocity and its generation mechanism, the analysis is implemented from the following perspectives. To begin with, slipstream velocity time traces at specified locations from the train vertical centerplane are processed to compute time-averages and standard deviations. The statistics are compared for the different cases. Next, *gust analysis* is conducted to understand the effect of ground motion on the maximum slipstream velocity defined by the TSI specification. The mechanism of how ground motion modifies slipstream is then examined by analysing the flow field at the prescribed slipstream assessment locations.

3.1.1. Analysis of unsteady statistics

According to the TSI specifications (European Union Agency for Railways, 2014), $U_{slipstream}$ is measured at 3 m away from the centre of the track and at two different heights (trackside height and platform height) above the top of the rails (TOR). The trackside and platform heights are 0.2 m ($z = 0.05H$) and 1.4 m ($z = 0.35H$) above the TOR, respectively. In this study, slipstream velocity measurements are collected for both heights between $-15H \leq x \leq 30H$. The time-average and standard deviation profiles of slipstream velocity ($U_{slipstream}$), together with the streamwise (U_{GF}) and spanwise (V_{GF}) velocity components at the two measurement heights, are presented in Fig. 4. The points corresponding to maximum values are listed in Table 3. Wind-tunnel measurements at the trackside height are included in Fig. 4 for comparison, noting the experimental set-up is comparable to the SGSW configuration. Fig. 4 shows a reasonably good agreement with the time-average profiles, and in the prediction of peak standard deviation. The potential reasons for the observed differences are discussed in the *Uncertainty Analysis* section of (Wang et al., 2017). In particular, that discussion presents reasons for the observed differences between the time-average profiles near the tail and beyond $x/H = 5$, which tend to be subject to higher experimental uncertainties, and the higher unsteadiness measured experimentally along the train, caused by background time-dependent wind-tunnel turbulence which probably also generates higher experimental slipstream readings further downstream.

Fig. 4 shows that in general ground motion has a significant impact on the slipstream predictions ($\overline{U}_{slipstream}$ and $\sigma_{slipstream}$), while the effect of wheel rotation is negligible. Here, $\overline{U}_{slipstream}$ represents a time-averaged slipstream velocity and $\sigma_{slipstream}$ its standard deviation. While the effect of ground motion is determined at both heights, its impact is greater at a lower height. Therefore, the following discussion in this section focuses on the trackside height results, unless stated otherwise. Qualitatively, similar trends of the $\overline{U}_{slipstream}$ profiles can be seen for the three cases. Local peak values occur near the nose and tail, and $\overline{U}_{slipstream}$ increases to a maximum behind the tail and then decreases gradually. This is a characteristic $\overline{U}_{slipstream}$ trend that has been observed across different train models and with various different techniques (Bell et al., 2016a), (Huang et al., 2016), (Baker, 2010), (Bell et al., 2015).

The peak value of $\overline{U}_{slipstream}$ in the wake is reduced and delayed due to the ground motion, which is consistent with the trend that was also identified by Xia et al. (2016a) based on the CRH3 model on a flat ground configuration. Due to the ground motion, the peak $\overline{U}_{slipstream}$ caused by the trailing vortices in the wake is reduced, while the local peak near the nose remains essentially identical. Consequently, the maximum $\overline{U}_{slipstream}$ for MGSG and MGRW configurations occurs at the nose, instead of within the wake. However, high $\sigma_{slipstream}$ still occurs within the wake region, with the maximum located at approximately $x = 5 \sim 6H$. Given this, the wake region is still the most critical region for HST slipstream assessment, and this is also identified by the gust analysis presented in Section 3.1.2.

Furthermore, by looking at the $\overline{U}_{GF}$ and $\overline{V}_{GF}$ variations, the results show that the main difference in $\overline{U}_{slipstream}$ between the three cases is mostly caused by the altered $\overline{U}_{GF}$ profile. Because the ground motion is in the streamwise direction, a moving ground removes the ground boundary-layer growth, which causes a high $\overline{U}_{GF}$ near the ground, and further affects the slipstream velocity. The mechanism of how the ground boundary-layer development influences slipstream is further explored in Section 3.1.3.

Table 3
The critical values in the slipstream profile comparison.

		$\overline{U}_{slipstream}$		$\sigma_{slipstream}$	
		Maximum	Location (x/H)	Maximum	Location (x/H)
Trackside	SGSW	0.116	6.61	0.081	5.61
	MGSW	0.078	−12.63	0.063	5.61
	MGRW	0.078	−12.63	0.063	5.61
Platform	SGSW	0.087	−12.57	0.046	7.55
	MGSW	0.088	−12.57	0.025	5.66
	MGRW	0.088	−12.57	0.026	18.06

3.1.2. Gust analysis

The TSI (European Union Agency for Railways, 2014) defines how the slipstream velocity should be measured under field testing, and the procedure for calculating the maximum slipstream velocity (also known as the TSI value) is briefly introduced here. The slipstream should be measured at two fixed positions: trackside height and platform height, as introduced before. The entire flow disturbance, including that caused by the train passing and the wake, needs to be recorded. Additionally, a 1-s moving-average (1s MA) filter is required to be applied to the raw data, and the peak slipstream velocity of the filtered data is recorded as one measurement. The distance between two independent measurements has to be more than 20 m, and a minimum of 20 independent measurements are required for calculating the maximum slipstream velocity (TSI value). The TSI value is calculated as the mean of the peak velocities plus two standard deviations. The TSI value notionally indicates the maximum slipstream velocity that is likely to occur at the measurement locations based on a 95% confidence interval, and this assessment is integrated into the HST acceptance procedure.

Numerically, *gust analysis* artificially replicates this full-scale testing procedure by utilising a *Moving Probe Technique*. This was originally applied to time-dependent velocity field data obtained from numerical simulation by Muld et al. (Muld et al., Henningson), to study slipstream under the TSI framework. A brief description of this gust analysis is presented here. Gust analysis requires a ground-fixed reference frame, while the numerical simulation utilises a train-fixed reference frame. Therefore, in order to replicate the ground-fixed environment, the first step is to place an artificial probe at the starting point of a slipstream measurement line, and then allow this probe to move downstream at the speed of U_∞. U_{GF} and V_{GF} are recorded during the time taken for the probe travelling from the start to the end point, and then $U_{slipstream}$ is calculated based on Eqn. (1), and plotted as grey solid curves in Fig. 5. To replicate the 20 m distance between individual measurements in a field-testing environment, the artificial moving probes are released every $5T_{\mathrm{ref}}$ (equivalent to 20 m at full scale). Thus, within the total simulation sampling time of $195T_{\mathrm{ref}}$, 58 independent measurements can be made (29 at each side), which satisfies the requirement of a minimum 20 independent measurements required for the TSI regulations (European Union Agency for Railways, 2014). The peak values of individual measurements are plotted as black dot points, and the mean ($\overline{U}_p$), and standard deviation (σ_{uv}) of the peak values are calculated and presented in Table 4. Next, the equivalent of a 1s MA filter is applied to each data set, and presented as light blue curves in Fig. 5, with the peak values indicated by the blue dot points. The final maximum slipstream velocity $\overline{U}_p + 2\sigma_{uv}$ under a 1s MA filter (TSI value) is calculated and presented in Table 4. In practice, the maximum value would be compared with the maximum allowable slipstream velocity specified under TSI as one part of the acceptance procedure. For this study, the duration of the equivalent sampling time per artificial probe is $52T_{\mathrm{ref}}$, with the starting and ending time for the train passage corresponding to $2.5T_{\mathrm{ref}}$ and $15.4T_{\mathrm{ref}}$, respectively.

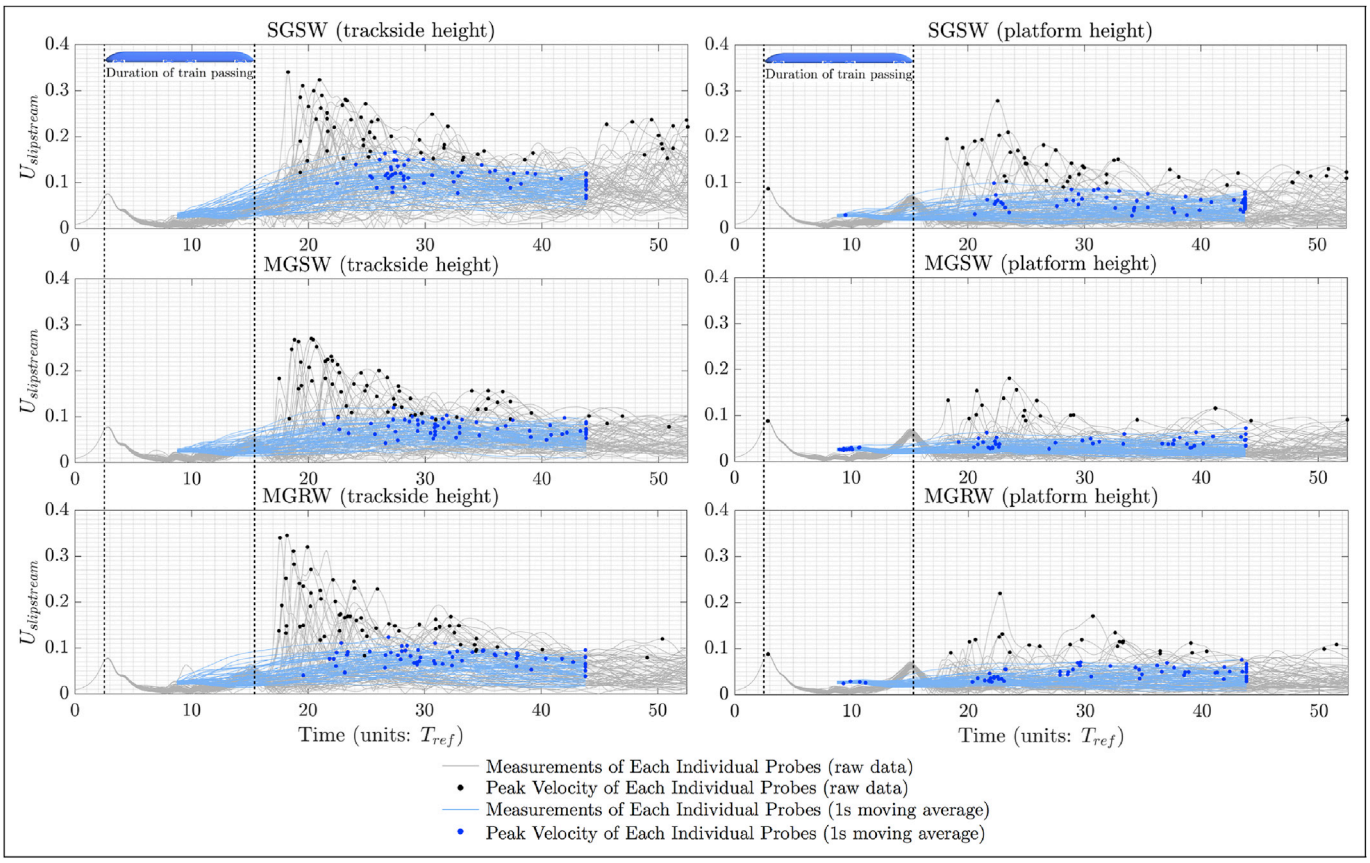

Fig. 5. The gust analysis based on the Moving Probe technique under TSI specifications.

Table 4
The unsteady statistics of gust analysis with and without 1s MA.

		Without 1s MA			With 1s MA		
		$\overline{U}_p$	σ_{uv}	$\overline{U}_p + 2\sigma_{uv}$	$\overline{U}_p$	σ_{uv}	$\overline{U}_p + 2\sigma_{uv}$
Trackside	SGSW	0.214	0.051	0.316	0.115	0.022	0.159
	MGSW	0.160	0.053	0.267	0.076	0.016	0.108
	MGRW	0.175	0.065	0.303	0.079	0.018	0.114
Platform	SGSW	0.126	0.041	0.208	0.055	0.016	0.088
	MGSW	0.098	0.020	0.138	0.039	0.011	0.061
	MGRW	0.100	0.023	0.145	0.045	0.013	0.072

Similar to full-scale testing (Baker et al., 2014) and moving-model experiments (Bell et al., 2015), the gust analysis shows a large run-to-run variance. Comparing measurements at trackside and platform heights, in general, the former shows a more identifiable peak at the near wake. The reason for this is that the high energy containing longitudinal vortices in the wake sit closer to the trackside position. More details about how the wake structures influence the slipstream measurement are presented in Section 3.2.

Additionally, for the SGSW probes at the trackside height a few measurements show a maximum $U_{slipstream}$ a long time after the passage of the tail, while this feature is not identified in MGSW and MGRW measurements. The high $U_{slipstream}$ in the far wake for the SGSW case is likely caused by ground boundary-layer growth, for which the mechanism is revealed in Section 3.1.3. These unrealistic high peaks in the far wake can affect the accuracy of gust analysis, not only in terms of the magnitudes of the maximum slipstream velocities (TSI value), but also their locations. Compared with the significant influence of ground motion, wheel rotation only has a slightly positive effect on the TSI value.

3.1.3. Flow field at the slipstream assessment location

According to the comparison in Sections 3.1.1 and 3.1.2, the ground motion has an effect on both the unsteady statistical profiles and maximum statistical slipstream velocity determination (the TSI value). In this section, the mechanism of how the ground motion alters slipstream is explained by examining the flow field at the slipstream measurement location (3 m away from the centreplane at full-scale).

The stationary ground introduces a streamwise shear between the ground and incoming air. This shear effect introduces y-vorticity (ω_y) into the flow field, and this can significantly alter the flow field near the ground and further affect the slipstream measurement, as illustrated in Fig. 6. The SGSW case shows a constant growth of positive $\overline{\omega}_y$ above the ground, where the overbar symbol indicates a time-averaged quantity. The moving ground removes the relative motion, and the altered $\overline{\omega}_y$ can be seen within the wake, which is covered by the ground boundary layer in the SGSW case. This alteration to $\overline{\omega}_y$ is purely introduced by the velocity difference between the wake propagation speed and the ground motion. The SGSW case shows a high unsteadiness of ω_y near the ground

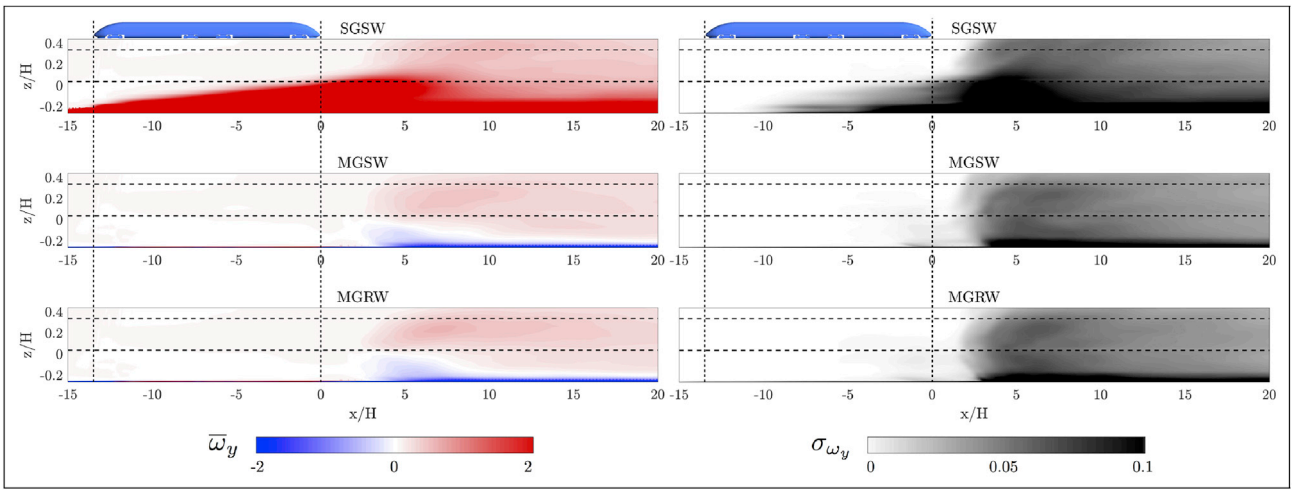

Fig. 6. $\overline{\omega}_y$ and σ_{ω_y} at the slipstream measurement location (Not to scale).

due to the ground boundary layer, while the MGSW and MGRW cases indicate that the high unsteadiness should predominately be caused by the wake, especially the region with an altered $\overline{\omega}_y$.

The influence on the slipstream measurement from the introduction of ω_y caused by the ground motion is illustrated in Fig. 7. The MGSW and MGRW cases show an identical $U_{slipstream}$ distribution, while the SGSW case shows a gradually increase of $\overline{U}_{slipstream}$ and $\sigma_{slipstream}$ near the ground, associated with the ground boundary layer. Fig. 7 shows that the ground boundary layer initially touches the trackside measurement line at approximately $x = 0H$, which is consistent with the location of the differences between the slipstream profiles plotted in Fig. 4. Additionally, Fig. 7 also explains why the ground motion effect is more significant at trackside height than at platform height, because the stationary ground imposes a local effect that is closer to the lower measurement line. Also, the ground boundary layer can alter the wake propagation and then affect the slipstream measurement. This mechanism is analysed further through the flow structures in Section 3.2.

3.2. Flow structures

In this section, for the ease of the discussion, the train-induced slipstream flow is split into two regions: flow development region and wake propagation region, as illustrated in Fig. 8. The flow development region is where the flow disturbance develops, while the wake propagation region covers where the developed flow structures propagate downstream. The classification is visualised in terms of $\overline{U}_{slipstream}$ at trackside height, as illustrated in Fig. 8, and the dashed lines indicate the positions of the slipstream measurements specified by TSI guidelines (European Union Agency for Railways, 2014). According to Fig. 8, it can be seen that the difference within the flow development region is negligible, while the SGSW case shows a wider wake in the wake propagation region.

The effect of the ground motion in each region is analysed in the following two subsections, and this approach aims to identify the effects of ground motion at each stage of slipstream development.

3.2.1. Flow development region

The flow development region is designated as the region where the flow develops as it passes over the HST model, which covers approximately from the nose to tail. The ground motion effect within this region is visualised by the time-averaged y-vorticity ($\overline{\omega}_y$) in the vertical spanwise centreplane ($y = 0W$), as shown in Fig. 9.

An identical boundary-layer development over the train top surface is indicated by the continuous growth of the positive $\overline{\omega}_y$ region. Compared with the MGSW and MGRW cases, the SGSW case shows a persistent thin positive $\overline{\omega}_y$ region above the ground surface due to the ground boundary layer. Even though the MGSW and MGRW cases have different wheel motion, the underbody flow fields are similar and consistent, with only minor differences observed around the axles.

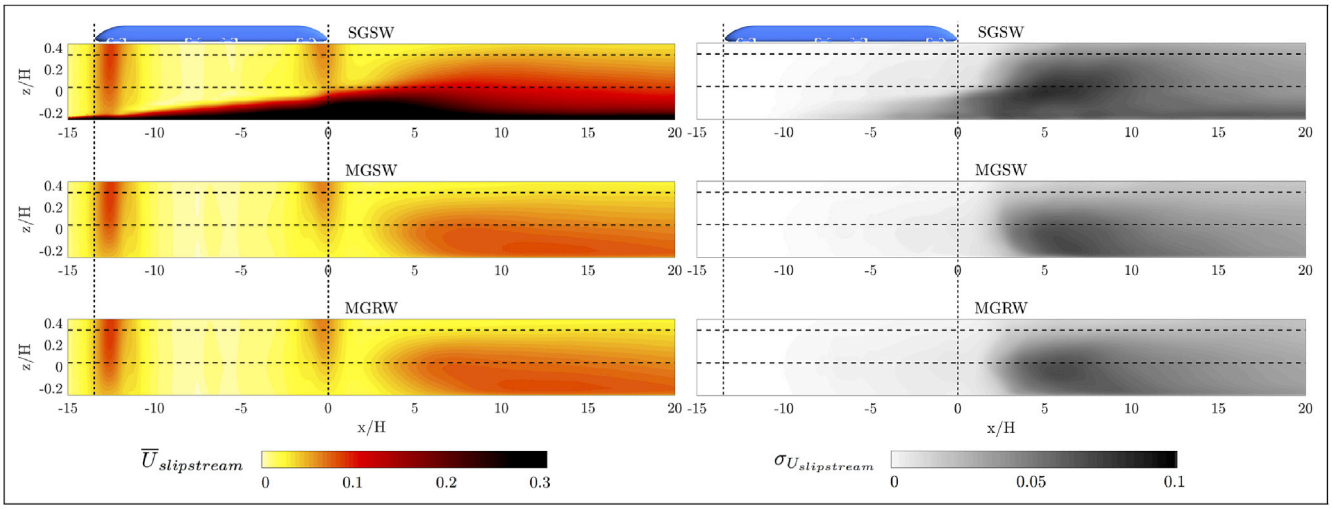

Fig. 7. $\overline{U}_{slipstream}$ and $\sigma_{U_{slipstream}}$ at the slipstream measurement location (Not to scale).

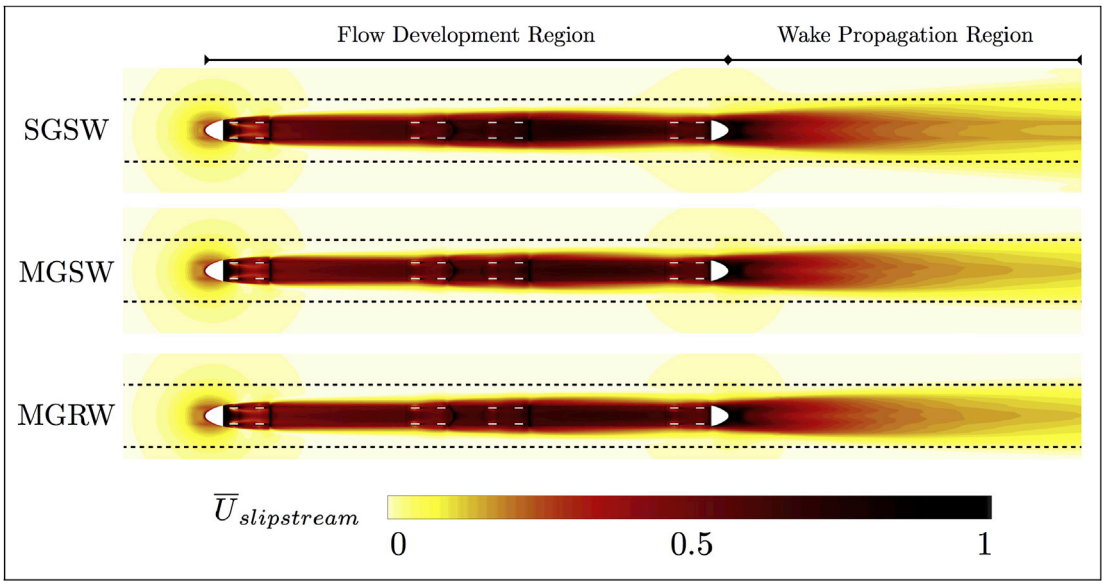

Fig. 8. The flow region classification visualised by $\overline{U}_{slipstream}$ at z = 0.05H.

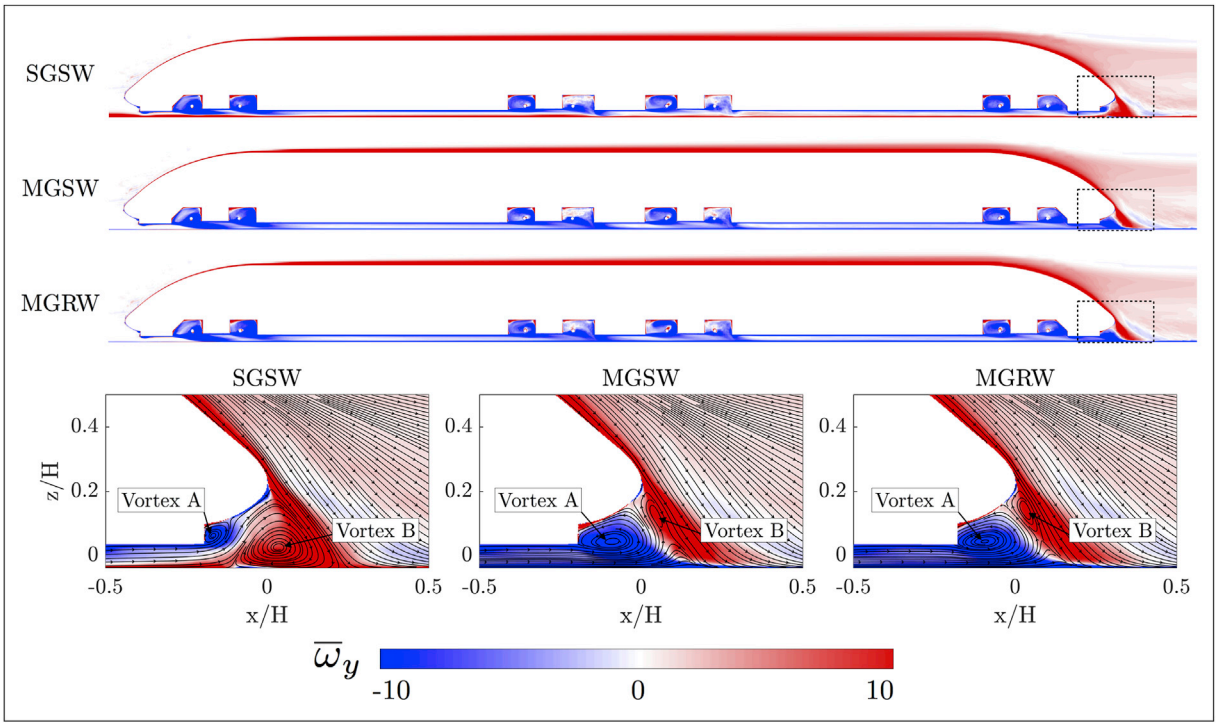

Fig. 9. The flow development region visualised by $\overline{\omega}_y$ and in-surface projected velocity streamlines at $y = 0W$.

A main alteration to the flow caused by ground motion occurs between the tail tip and the ground, as highlighted in Fig. 9. According to the $\overline{\omega}_y$ and in-surface projected velocity streamlines, two coherent recirculation regions (vortex A and B) are formed when the downwash from the top surface meets the underbody flow. From the density of the streamlines, the velocity of the underbody flow in the SGSW case is significantly lower than that in the MGSW and MGRW cases. Compared with the latter cases, when the underbody flow meets the downwash from the tail, the SGSW case has relatively lower kinetic energy that can be used to drive the production of the large vortex (vortex A). Additionally, although the size of vortex A varies significantly between the stationary and moving ground cases, the position of the outside boundary of the vortex B slightly further downstream shows little variation.

3.2.2. *Wake propagation region*

The wake propagation region is designated as the region behind the tail, where the vortical flow structures separate from the train surface and move downstream. According to the slipstream profiles presented in Section 3.1, ground motion has a significant impact on the slipstream velocities recorded within the wake propagation region. To investigate the interaction between the ground motion and wake propagation, both the time-averaged and transient flow structures are analysed.

Similar to the flow structures that have been identified from previous studies (Bell et al., 2016a) (Bell et al., 2016b), the dominant feature of a

HST wake is a pair of counter-rotating streamwise vortices. In this study, the time-averaged wake is visualised by x-vorticity (ω_x) contours overlaid with in-surface projected velocity streamlines on five sequential vertical planes, as illustrated in Fig. 10. As the time-averaged flow structure is symmetric about the mid-plane, only the left half of the flow field is presented. The black crosses and circles in Fig. 10 represent the locations of trackside ($z = 0.05H$) and platform ($z = 0.35H$) slipstream measurement positions.

Through Fig. 10, the downstream evolution of the time-mean trailing vortices can be visualised as the plane is shifted from $x = 0.5H$ to $x = 6H$. Qualitatively, the three cases present an identical flow feature: as the vortices move downstream, they roll over the rails and move apart from each other in the spanwise direction. Quantitatively, due to the presence of ground boundary layer, the SGSW case shows a negative x-vorticity region above the ground that deforms the shape of trailing vortex. Comparing with MGSW and MGRW cases, the trailing vortex merges into the ground boundary-layer region, resulting in the lower end of the vortex shifting closer to the trackside slipstream measurement location. As the vortex core contains lower momentum fluid, it induces a higher local slipstream velocity. Therefore, the slipstream velocity is sensitive to both the strength of the trailing vortex arms and their cross-stream location. As the vortex is deformed towards the trackside slipstream measurement line, the SGSW setup implies a higher slipstream measurement compared with the MGSW and MGRW setups, which is another reason why the SGSW case shows a higher prediction of $\overline{U}_{slipstream}$.

The transient wake structure is illustrated by phase-averaging $U_{slipstream}$ over a horizontal plane at the trackside height, and the shedding frequency is quantified by the Strouhal number (St_W) based on the train width (W) and streamwise velocity component (U_{TF}) at the point $(1H, -0.4W, 0.2H)$. The power spectra are presented in Fig. 11. The signal is split into 26 segments filtered with Hanning windows with 25% overlap for each fast Fourier transform to construct the overall spectra and highlight the dominant frequencies. According to Fig. 11, the dominant near wake St_W is approximately 0.22, 0.4–0.6 and 0.55 for the SGSW, MGSW and MGRW cases, respectively. This indicates that the wake oscillates more rapidly with a moving ground. The ground boundary layer reduces the longitudinal velocity in the wake region above the ground, as is clear in Fig. 4. This also explains why the SGSW case demonstrates a cleaner peak, while the MGSW and MGRW cases show a wider bandwidth towards higher St_W values.

The spanwise wake oscillation that has been identified in the wind-tunnel experiments of (Bell et al., 2016b), is visualised by phase-averaging $U_{slipstream}$ in a horizontal plane at the trackside height ($z = 0.05H$), as presented in Fig. 12. In Fig. 12, the black dashed lines indicate the location of slipstream assessment locations according to TSI standards (European Union Agency for Railways, 2014), and phase-averaging is conducted based on the signal at the reference point with coordinates $([2H, -0.5W, 0.05H])$, visualised by the blue circles in Fig. 12. The first and second row demonstrate the wake motion that is half a period apart, and the third row illustrates snapshots of the instantaneous wake structure for the three cases. Comparing with the MGSW and MGRW cases, both the phase-averaged and instantaneous wake profiles demonstrate that a stationary ground enhances the amplitude of the spanwise wake oscillation. Additionally, Fig. 12 also implies that due to the ground boundary-layer development, the side-to-side oscillation is enhanced with distance downstream. Longitudinally, all the cases predict the same longitudinal wavelength of $2.5 \sim 3H$, showing no significant dependency on the ground motion.

The spanwise motion is also quantified by the cross-correlation of a pair of point arrays within the near wake, as visualised by the white crosses in Fig. 12. The points are distributed between $x = 0 \sim 5H$ in $0.5H$ increments, and each pair is $0.5W$ from the centreplane. The cross-correlation coefficient of V_{GF} for each pair is calculated, and the average profile of 11 pairs for each case is plotted in Fig. 13. The cross-correlation coefficient of unity represents an in-phase motion, while -1 means an out-of-phase motion, and the time lag is normalised by T_{ref}. Thus, an ideal in-phase spanwise motion should have a cross-correlation coefficient for V_{GF} equal to 1. Fig. 13 shows the coefficients for the SGSW case at zero time lag is approximately 0.205, approximately double the values recorded for the MGSW and MGRW cases that are about 0.1. This is in line with the phase-averaging analysis, which shows a more identifiable spanwise wake oscillation for SGSW. Additionally, the temporal period of the half spanwise motion, determined by the time lag between the positive and negative peak values, is approximately $2T_{\text{ref}}$, independent of the ground motion.

The amplification of the spanwise motion is caused by the deformation of the vortex pair as it interacts with the ground boundary layer while advecting downstream. As presented in Fig. 10, this deformation causes a wider wake, especially towards the lower part. In contrast, the vortices stay closer to the centreplane for the moving ground cases with the absence of the ground boundary-layer influence. Additionally, the spanwise oscillation is orthogonal to the longitudinal ground boundary-layer development, and it seems that the longitudinal ground motion does not alter the spanwise wake oscillation frequency to any significant effect. In conclusion, from the phase-averaging and cross-correlation results, the ground boundary layer enhances the amplitude of the spanwise motion, while the spatial wavelength and temporal period of the spanwise oscillation are effectively independent of ground motion.

3.3. Aerodynamic loading

The aerodynamic (pressure) loading on the train surface is visualised through the Pressure Coefficient (C_P) distribution as presented in Fig. 14, where C_P is defined by

$$C_P = \frac{P - P_\infty}{\frac{1}{2}\rho_\infty V_\infty^2}. \tag{3}$$

Here, P is the surface pressure, and reference values for the pressure, density and velocity are P_∞, ρ_∞ and V_∞, respectively. In CFD simulations, P_∞ is typically set as the static pressure at the domain outlet, which is zero in this study. Quantitatively, the differences between the C_P distributions are almost negligible, especially on the top surface. Not surprisingly, the main differences occur along the bottom surface, especially around the bogie regions. Even though almost qualitatively identical pressure distributions are established; quantitatively the moving ground generates a higher pressure deviation on the underbody structures, and wheel rotation causes extra higher pressure deviations on the wheels and axles. The C_P variation on the bottom surface is clearly caused by the different underbody flow conditions. The boundary layer on the stationary ground reduces the underbody flow velocity; therefore, the impact of the incoming flow on the underbody structures is reduced. Compared with the ground motion effect that is exerted over the entire bottom surface, the wheel rotation only increases the pressure magnitude around the wheel sets, due to further acceleration of the local flow field introduced by the wheel rotation. This difference can also be identified from the pressure profiles on the train centreplane, as shown in Fig. 15.

From the C_P distribution over the train surface, both the drag (C_D) and lift (C_L) coefficients are calculated and listed in Table 5. The ground motion alone increases C_D from 0.267 to 0.281 (5.1%), while wheel rotation produces another 0.7% increase. The ground motion causes a more significant impact in the vertical direction, resulting in an up to 50% reduction of C_L. The higher C_D for the moving ground cases is a result of the greater impact between the incoming flow and underbody structures. Additionally, the underbody flow acceleration reduces the velocity difference between the flow over the top and bottom surface, resulting in a smaller pressure difference in the vertical direction, hence the reduction of C_L. A slightly higher standard deviation is determined for both C_D and C_L with the stationary ground, which is introduced by the unsteadiness of the ground boundary layer. Additionally, wheel rotation can be another minor source of unsteadiness.

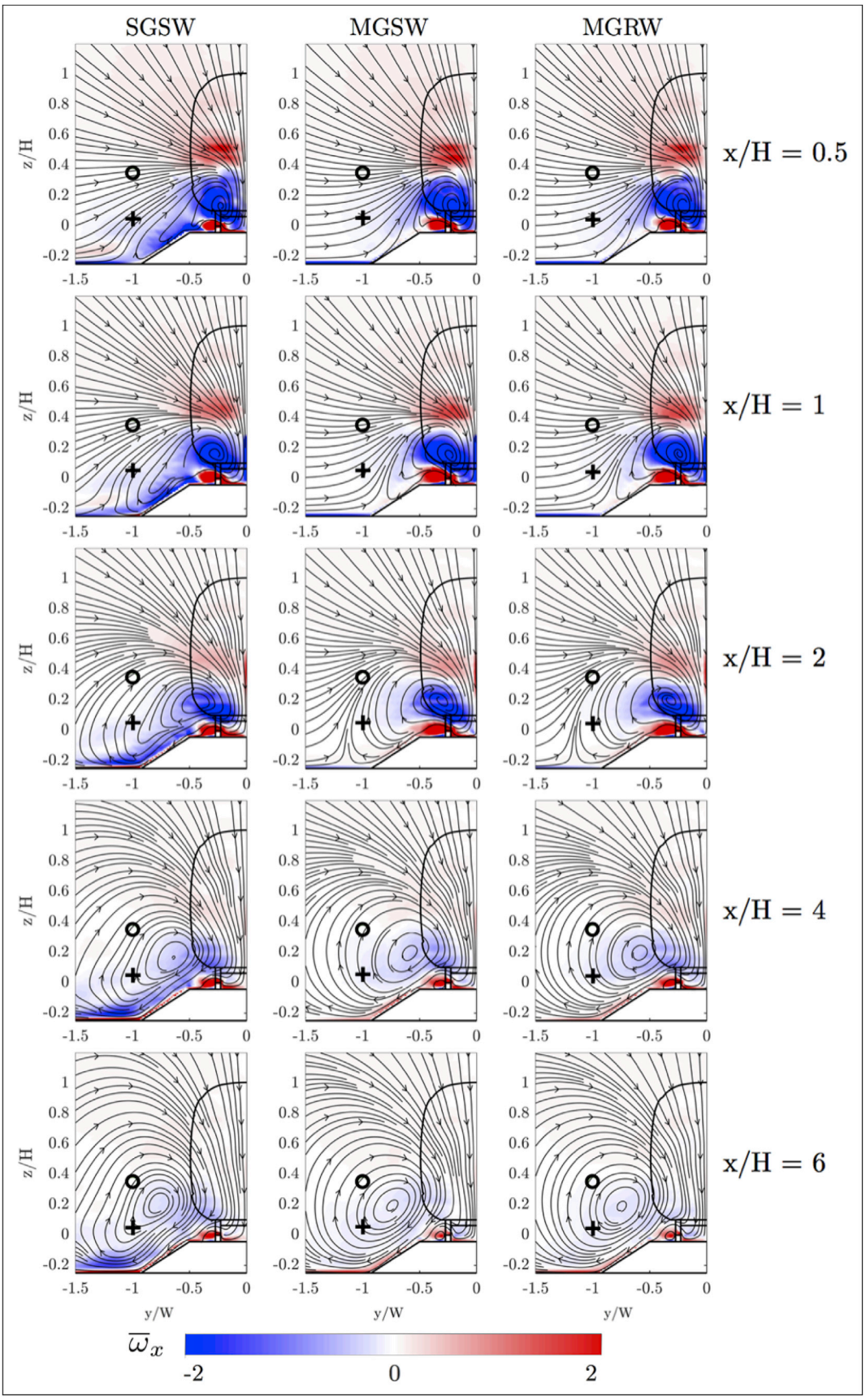

Fig. 10. The time-averaged wake structure visualised by ($\overline{\omega}_x$) coloured contours and in-surface projected velocity streamlines (+: trackside measurement location; o: platform measurement location).

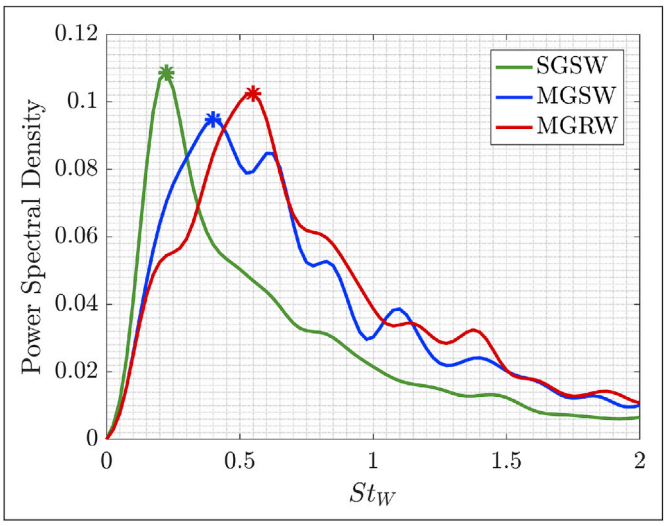

Fig. 11. The comparison of wake shedding frequency based on St_W at the point of $[1H, -0.4W, 0.2H]$.

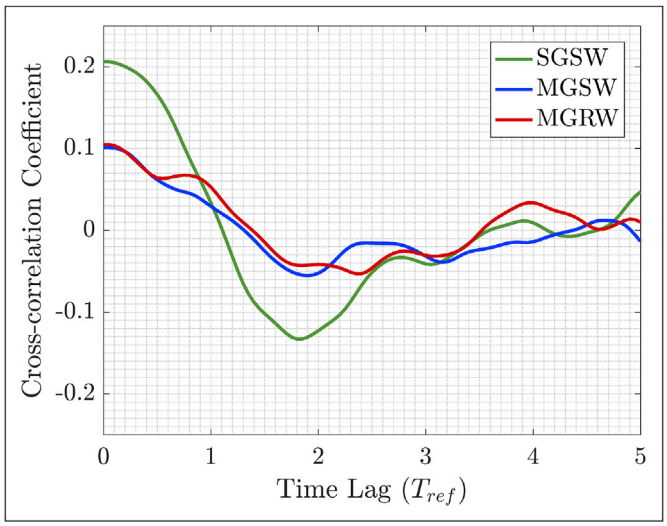

Fig. 13. The cross-correlation coefficient comparison of the spanwise wake oscillation.

4. Conclusion

In this study, based on three different wheel and ground configurations (SGSW, MGSW and MGRW), the effects of the ground motion on a HST slipstream are investigated from the perspectives of the slipstream assessment, wake structure and aerodynamic loading. This study not only determines the alteration to slipstream due to ground motion, but also explores the mechanism of how ground motion affects slipstream by analysing the time-averaged wake structure and wake dynamics. In terms of slipstream assessment, a stationary ground increases both $\overline{U}_{slipstream}$ and $\sigma_{slipstream}$, especially in the wake region at a lower height above the ground. This is in line with the gust analysis that shows that the presence of a ground boundary layer can result in an over-prediction of the maximum slipstream velocity (TSI value).

The ground motion affects slipstream both directly and indirectly. Directly, a stationary ground increases the slipstream velocity $U_{slipstream}$ in the wake due to the difference in the ground and air velocities causing lower wake velocities relative to the train. Indirectly, the spreading of the longitudinal trailing vortices due to the interaction between the wake and ground boundary layer results in a wider wake structure. Additionally, the side-to-side deformation of the longitudinal trailing vortices due to the interaction between the wake and ground boundary layer results in

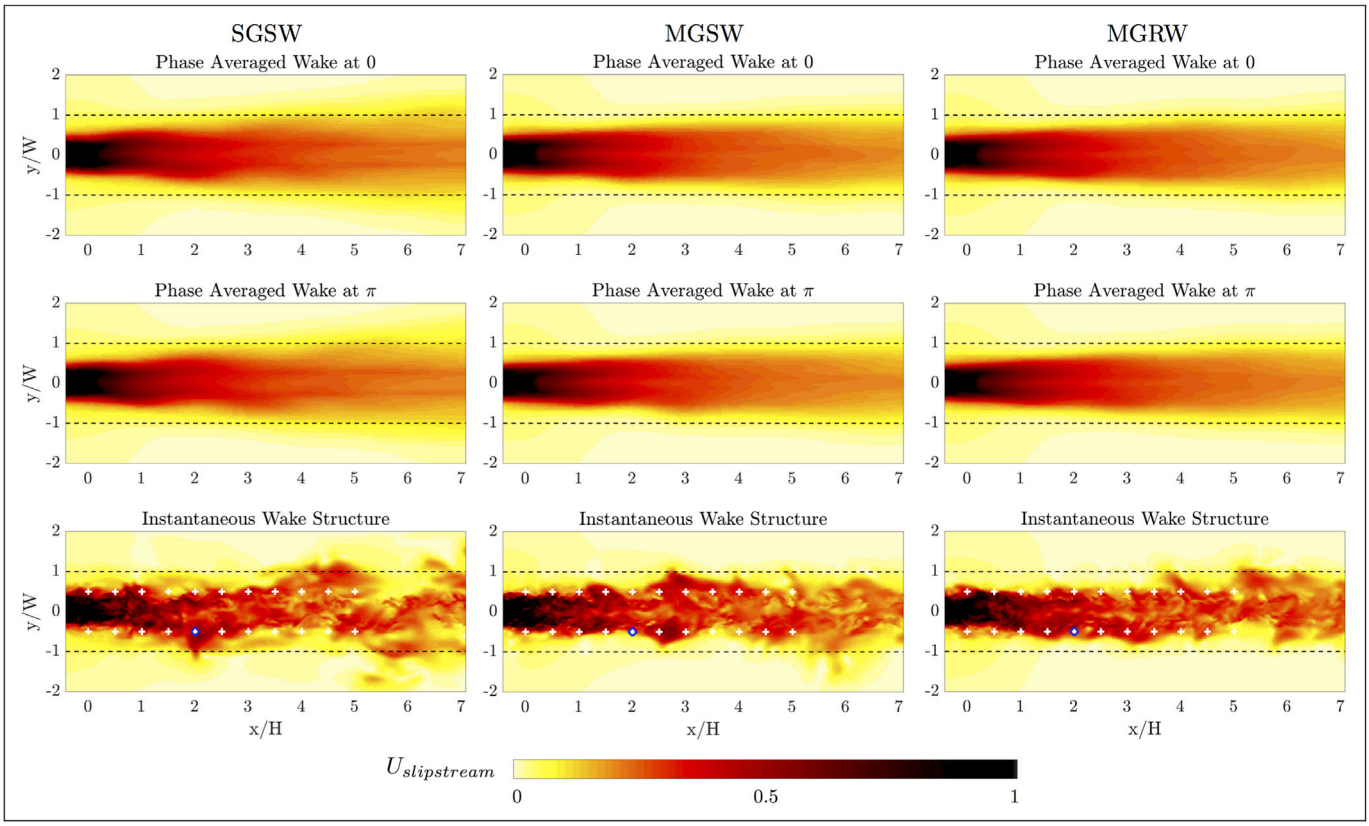

Fig. 12. The wake dynamics visualised by the phase-averaged and instantaneous $U_{slipstream}$ at Rz = 0.05HR (o: phase-averaging reference points; +: cross-correlation points).

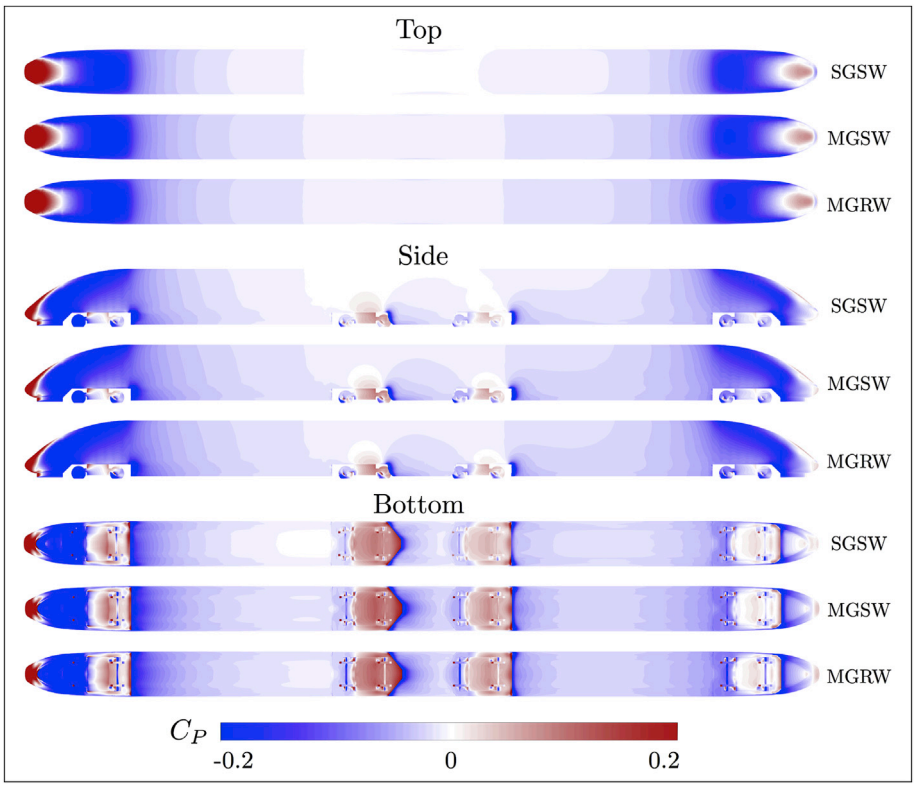

Fig. 14. The comparison of train surface pressure coefficient.

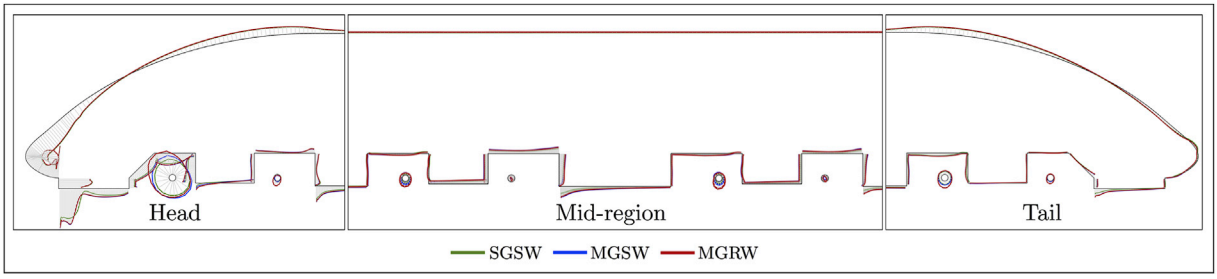

Fig. 15. The comparison of surface pressure coefficient profile at the train centreline.

Table 5
The comparison of force estimation on the train.

		SGSW	MGSW	MGRW
C_D	Mean	0.267	0.281	0.283
	Standard deviation	0.010	0.008	0.009
C_L	Mean	0.083	0.049	0.051
	Standard deviation	0.017	0.015	0.016

a trailing vortices meandering further from the train vertical centreplane, causing increased gusts; and the amplitude increases as the wake propagates downstream. Dynamically, both the streamwise wavelength and temporal period of the spanwise motion are not affected by the ground boundary layer, while the wake shedding frequency is increased with a moving ground. The major ground motion effect within the flow development region is the alteration of the sizes of two coherent vortices between the tail tip and ground, caused by the different underflow conditions. For the aerodynamic loading, a stationary ground predicts a lower C_D and a higher C_L, mainly caused by the train bottom surface pressure alteration due to the variation to the underflow conditions caused by the ground boundary. Additionally, the wheel rotation only alters the local flow field and pressure distribution within the bogie region; its effect on the slipstream assessment and wake structures are limited.

Note that in order to try to isolate the effect of the ground boundary condition on the slipstream and aerodynamic forcing, the present study is based on a reduced-length partially de-featured HST model. Both an increase in train length and the addition of more realistic underbody features may alter the details of predicted flow features. In particular, increased underbody complexity is likely to have a non-negligible effect on the calculated drag and also on the difference in the drag predictions between the stationary and moving ground cases.

References

Ambrósio, J., Pombo, J., Pereira, M., Antunes, P., Mósca, A., 2012. A computational procedure for the dynamic analysis of the catenary-pantograph interaction in high-speed trains. J. Theor. Appl. Mech. 50 (3), 681–699.
Baker, C., 2010. The flow around high speed trains. J. Wind Eng. Industrial Aerodynamics 98, 277–298.
Baker, C.J., Quinn, A., Sima, M., Hoefener, L., Licciardello, R., 2014. Full-scale measurement and analysis of train slipstreams and wakes. part 2 gust analysis. Proc. Institution Mech. Eng. Part F J. Rail Rapid Transit 228 (5), 468–480.

Bell, J.R., Burton, D., Thompson, M.C., Herbst, A.H., Sheridan, J., 2014. Wind tunnel analysis of the slipstream and wake of a high-speed train. J. Wind Eng. Industrial Aerodynamics 134, 122–138.
Bell, J.R., Burton, D., Thompson, M.C., Herbst, A.H., Sheridan, J., 2015. Moving model analysis of the slipstream and wake of a high-speed train. J. Wind Eng. Industrial Aerodynamics 136, 127–137.
Bell, J.R., Burton, D., Thompson, M.C., Herbst, A.H., Sheridan, J., 2016. Flow topology and unsteady features of the wake of a generic high-speed train. J. Fluids Struct. 61, 168–183.
Bell, J.R., Burton, D., Thompson, M.C., Herbst, A.H., Sheridan, J., 2016. Dynamics of trailing vortices in the wake of a generic high-speed train. J. Fluids Struct. 65, 238–256.
Bell, J., Burton, D., Thompson, M., Herbst, A., Sheridan, J., 2017. A wind-tunnel methodology for assessing the slipstream of high-speed trains. J. Wind Eng. Industrial Aerodynamics 166, 1–19.
Burgin, K., Adey, P., Beatham, J., 1986. Wind tunnel tests on road vehicle models using a moving belt simulation of ground effect. J. Wind Eng. Industrial Aerodynamics 22 (2), 227–236.
DIN Standards Committee Railway/Normenausschuss Fahrweg und Schienenfahrzeuge (FSF), http://www.fsf.din.de (2014).
European Union Agency for Railways, 2014. Commission Regulation (EU) No 1302/2014 Concerning a Technical Specification for Interoperability Relating to the 'rolling Stock — Locomotives and Passenger Rolling Stock' Subsystem of the Rail System.
Fago, B., Lindner, H., Mahrenholtz, O., 1991. The effect of ground simulation on the flow around vehicles in wind tunnel testing. J. Wind Eng. Industrial Aerodynamics 38 (1), 47–57.
Huang, S., Hemida, H., Yang, M., 2016. Numerical calculation of the slipstream generated by a crh2 high-speed train. Proc. Institution Mech. Eng. Part F J. Rail Rapid Transit 230 (1), 103–116.
Krajnović, S., Davidson, L., 2005. Influence of floor motions in wind tunnels on the aerodynamics of road vehicles. J. Wind Eng. Industrial Aerodynamics 93 (9), 677–696.
Krajnović, S., Ringqvist, P., Nakade, K., Basara, B., 2012. Large eddy simulation of the flow around a simplified train moving through a crosswind flow. J. Wind Eng. Industrial Aerodynamics 110, 86–99.
Kwon, H.-b., Park, Y.-W., Lee, D.-h., Kim, M.-S., 2001. Wind tunnel experiments on Korean high-speed trains using various ground simulation techniques. J. Wind Eng. Industrial Aerodynamics 89 (13), 1179–1195.
Mizushima, F., Takakura, H., Kurita, T., Kato, C., Iida, A., 2007. Experimental investigation of aerodynamic noise generated by a train-car gap. J. Fluid Sci. Technol. 2 (2), 464–479.
T. W. Muld, G. Efraimsson, D. S. Henningson, Mode decomposition and slipstream velocities in the wake of two high-speed trains, Int. J. Railw. Technol. ISSN 2049-5358, E-ISSN 2053-602X..
Railway Applications, 2013. Aerodynamics Part 4: Requirements and Test Procedures for Aerodynamics on Open Track, CEN EN 14067–4.
Sardou, M., 1986. Reynolds effect and moving ground effect tested in a quarter scale wind tunnel over a high speed moving belt. J. Wind Eng. Industrial Aerodynamics 22 (2–3), 245–270.
Shuanbao, Y., Dilong, G., Zhenxu, S., Guowei, Y., Dawei, C., 2014. Optimization design for aerodynamic elements of high speed trains. Comput. Fluids 95, 56–73.
Spalart, P.R., 2009. Detached-eddy simulation. Annu. Rev. fluid Mech. 41, 181–202.
Wang, S., Bell, J.R., Burton, D., Herbst, A.H., Sheridan, J., Thompson, M.C., 2017. The performance of different turbulence models (urans, sas and des) for predicting high-speed train slipstream. J. Wind Eng. Industrial Aerodynamics 165, 46–57.
Xia, C., Shan, X., Yang, Z., 2016. Influence of ground configurations in wind tunnels on the slipstream of a high-speed train. In: 8th International Colloquium on Bluff Body Aerodynamics and Applications. Northeastern University, Boston.
Xia, C., Shan, X., Yang, Z., 2016. Comparison of different ground simulation systems on the flow around a high-speed train. Proc. Institution Mech. Eng. Part F J. Rail Rapid Transit, 0954409715626191.
Zhang, J., Li, J., Tian, H., Gao, G., Sheridan, J., 2016. Impact of ground and wheel boundary conditions on numerical simulation of the high-speed train aerodynamic performance. J. Fluids Struct. 61, 249–261.